AIAA SciTech Forum
8-12 January 2024, Orlando, FL
AIAA SCITECH 2024 Forum

10.2514/6.2024-2367

Methods for Mitigating Backsputter in Electric Propulsion Test Facilities I: Beam Halter Concept and Design

Seth J. Thompson[1], Jack P. Garman[2], Zach C. Robertson,[3] and John D. Williams[4]
Colorado State University, Fort Collins, CO, 80523, USA

Will Hurley[5], Tate Gill[5], Collin B. Whittaker[5], and Benjamin A. Jorns[6]
University of Michigan, Ann Arbor, MI, 48109, USA

This work presents a concept for reducing backsputter to thrusters from a test facility beam target and wall. The concept is referred to as a Hall thruster in reverse (Halter), and it uses a transverse magnetic field applied using a high transparency picket-fence configuration of permanent magnets with a positively biased plate buried within the structure for slowing beam ions thus reducing sputtering while the transverse field restricts the flow of electrons from the beam plasma to the plate preventing the Halter from perturbing thruster operation. The basics of the transverse magnetic field configuration and the sputter mitigation concept are explained, and its expected effectiveness in terms of reduced backsputter to the thruster is explored using two models—one model is used to predict backsputtering from the Halter, and a separate model is used to predict the ion and electron currents flowing to the buried plate. The target sputter model is exercised to estimate the effectiveness of the Halter across plate biases and background pressures, while the I-V model is used to fit experimental measurements of a small-scale prototype. Measurements of the prototype tested in the beam of a gridded ion source as a function of the buried plate voltage, beam ion energy, and axial position relative to the ion source are presented. At low plate biases net ion current is detected, and the current decreases with increasing plate bias as beam plasma electrons cross the transverse field region to reach the buried plate. It was observed that the Halter plate floating potential increased as the Halter prototype was moved axially away from the ion source to regions of lower ion beam current density and plasma density. The model developed to fit the I/V characteristics of the Halter plate for the given beam and plasma properties at its entrance is used to provide insight into improving the concept. A figure of merit of the Halter is the floating potential of the buried plate—high floating potentials imply significantly slowed ions and reduced sputtering while minimizing perturbations of the Halter on electrical interactions between the thruster and the test facility. We have found that the prototype Halter can achieve floating potentials within 80% of the beam ion energy if the plasma density at its entrance is held to a sufficiently low value, but when it is placed closer to the gridded ion source in a region of higher plasma density, the floating potential of the buried plate is only tens of volts above the beam plasma potential.

[1] Research Associate, Mechanical Engineering, seth.thompson9@gmail.com
[2] Undergraduate Research Assistant, Mechanical Engineering
[3] Graduate Research Assistant, Mechanical Engineering
[4] Professor, Mechanical Engineering.
[5] Graduate Research Assistant, Aerospace Engineering
[6] Associate Professor, Aerospace Engineering

I. Introduction

The desired long lifetime of electric propulsion (EP) devices has rendered full-length lifetime qualification tests impractical in terms of both time and available funding—and very high-power thrusters are making ground-based testing even more unfeasible due to the requirements for increased vacuum chamber size and pumping capacity to avoid excessive test facility background pressures and excessive thruster contamination from sputtering of the chamber beam target and wall. As a result, a premium has been placed on developing models and using them to interpret performance and erosion rates measured during limited-duration testing at higher-than-desired facility pressure under conditions of elevated backsputter rates. The hope is that the models could be used to predict performance and lifetime expected in space. The success of this strategy would negate the need to operate the device to end-of-life in ground-based qualification testing.

There are concerns about the fidelity of the limited-duration, ground-based tests and the ability to use these results to predict in-space performance and lifetime. In both gridded ion and Hall thrusters, sputter erosion of the devices that results from the operation of the device itself is considered to be their life-limiting mechanism. To quantify this, limited-duration wear tests are often utilized to determine the erosion rates of life-limiting components [1], [2]. This process of measuring erosion of the thruster through limited-duration testing can be significantly impacted by the deposition of sputtered material from facility surfaces onto the thruster, often referred to as the backsputter of the facility. This rate has been estimated to be on the order of the erosion rate in 12.5kW Hall thruster tests [3], which will worsen as power is scaled up into the 100 kW range. Furthermore, accelerated testing performed with beam targets placed closer to the thruster, where backsputter rates are significantly increased, discovered that the film growth rate of the backsputtered material will likely stymie limited-duration wear tests performed at high power [4]. This problem is only further exacerbated by increases in EP device power that produce higher current and/or energetic beams that further increase the rate of backsputter to the thruster [5]–[7]. Lastly, increased demand for lower-cost propellants has resulted in efforts to qualify EP devices on krypton and argon gasses that are expected to have enhanced sputter rates due to better momentum transfer as sputter targets, usually carbon, and propellant ion atomic masses grow more similar [8]. While higher fidelity models are being developed to quantify this effect [9], experimental efforts like the one presented herein are underway to mitigate the problem and provide useful datasets for model validation efforts.

Approaches to reduce the backsputter rate of the thruster under test have been explored for some time, with the use of graphite, a low sputter yield material, and angled beam dump designs being standard practice in many high-power EP test facilities [10]. New approaches for reducing backsputter, such as using volumetrically complex materials (VCMs) to trap sputtered particles in the materials themselves, are also being explored [11]. Numerical simulation of surface morphology evolution has shown initial sputter yield reduction under normal incident ion bombardment of textured surfaces [12]. It is still unclear if these materials will be feasible to scale to the sizes needed for large vacuum facilities or if they will retain a low sputter yield throughout a limited-duration test.

An active mitigation approach would be to slow down the incident beam ions before they impact surfaces through the use of electric fields. Previous tests have explored the effect of biasing a large area beam dump with respect to chamber ground to determine its effect on the thruster operation [13]. This testing revealed increases in beam plasma potential and collection of amperes of beam plasma electrons commensurate with the magnitude of the bias applied to the beam dump. This would therefore have little to no effect on the backsputter rate to the thruster as ions generated at potentials higher than the plume plasma would still arrive at the surface with sufficient energy to sputter the beam target. To mitigate this effect, we proposed an active mitigation strategy that uses electric and/or magnetic fields to slow incoming ions and shield electric fields from affecting plume properties, thereby limiting the effects of the bias applied to a downstream surface on thruster and beam plasma properties. This system could be considered a “beam catcher” that slows the incoming ions but limits any interaction with the thruster, the beam plasma, and the test facility.

A. Beam Catcher Concepts

Two concepts for catching beam ions are the “ion thruster in reverse” and the “Hall thruster in reverse” (Halter) back sputter mitigation systems. These devices can be configured in several ways, and examples of both the ion thruster in reverse and the Halter concepts are shown in Figure 1. These devices operate using grounded grid plates and magnets, or electron retarding plates, with appropriate spacing to limit the direct coupling of plume electrons to the positively biased ion energy suppression plate. The permanent magnets shown for the Halter concept in Figure 1 (right) are shielded by a grounded plate made from graphite. The line of magnets, grounded plates, and suppression plates are assumed to extend into the page. This configuration of the Halter design is referred to as a “picket-fence” magnetic

configuration and relies on magnets to produce a sufficiently strong transverse magnetic field across the surface of the ion energy suppression plate to limit plume electrons from arriving at the plate surface.

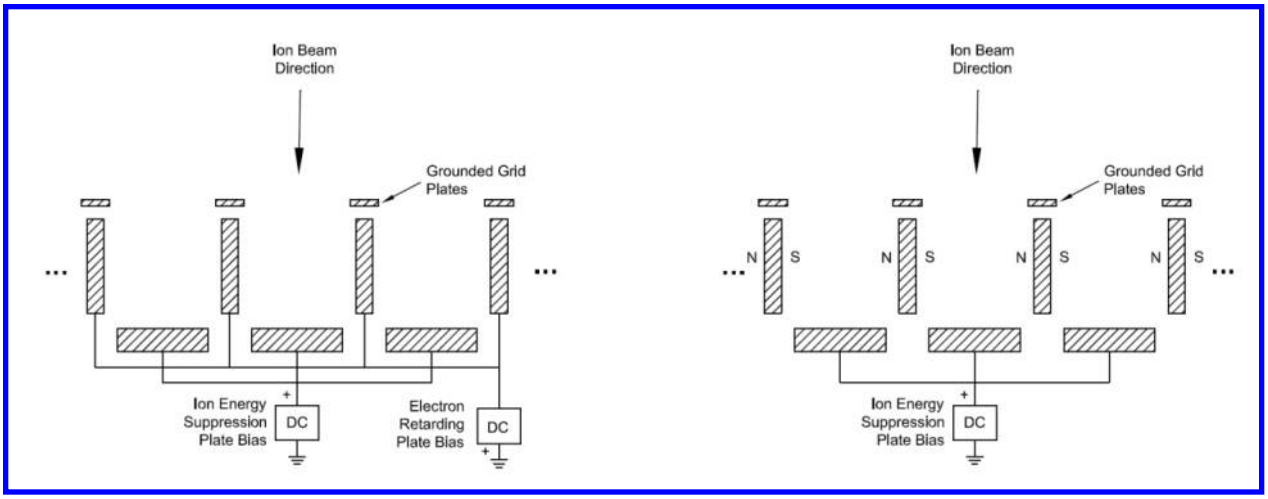

Figure 1: Ion thruster in reverse (left) and Hall thruster in reverse (right) shown in a picket fence configuration with cross-sections assumed to extend into the page.

The grounded grid plates in Figure 1 would still be sputtered by particles with the full ion beam energy, but ions that flow in between the grid plates would be slowed by the electric field between the suppressor plate and plume plasma before arriving at the plate surface. Ideally, this potential could be set to near that of the anode voltage in a Hall thruster to slow most incoming ions to energies below the sputter threshold of the plate material. However, there may be a limit to the applied plate bias before interaction with the beam plasma occurs. However, the precipitous drop of sputter yield of many materials at low energies [14], [15] indicates that decreasing the incoming ion energy by only a modest fraction may be all that is necessary to decrease the backsputter rates to more acceptable levels.

Another configuration of the Halter concept is to utilize the applied magnetic field from solenoidal structures placed around or beneath the ion energy suppression plate. The applied magnetic field from a solenoid may eliminate or drastically reduce the exposed area of grounded support structures and grid plates that can be sputtered by incoming ions. Figure 2 shows a diagram of this Halter configuration with no grounded surfaces over the ion energy suppression plate and with solenoidal structures assumed to be out of the beam with no shadowing of the ion energy suppression plate required. Eliminating the ground plates may simplify construction while enabling variable magnetic field strengths to be tested, aiding in characterization efforts.

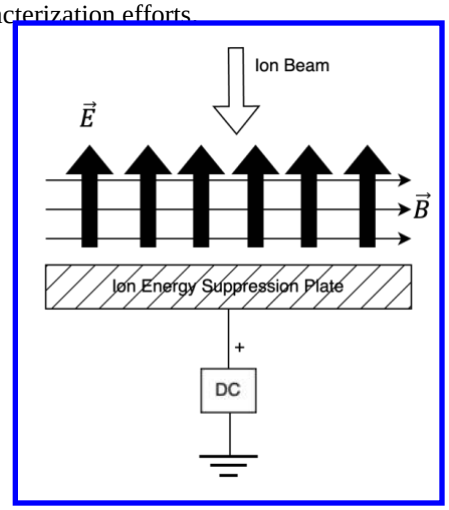

Figure 2: Representative schematic of an induced magnetic field Halter system.

The expected effectiveness of these backsputter mitigation concepts will be influenced by several factors, such as the open area fraction between the grounded grid plates in the picket fence configuration, the magnetic field strength, the bias of the ion energy suppression plate, and the neutral background pressure, to name a few. An approach for evaluating the strength that each factor has on overall effectiveness of reducing backsputtering is developed below in Section III.A. For a beam catcher concept to be feasible, it must be shown that the sputter mitigation strategy employed has limited or no impact on test fidelity via plume interactions or other thruster effects. We explore these topics by applying a simplified Halter model and a scaled prototype operated downstream of a gridded ion source. Section II describes the picket fence Halter prototype and the gridded ion test facility, while Sections III.A and III.B describe the models that we employed to determine expected effectiveness and guide further development. This includes a description of the expected backsputter reduction under various conditions and a simplified model used for fitting the collected current versus applied voltage of the ion energy suppression plate of our prototype Halter. Section IV describes the results of these simulations and preliminary prototype testing in the beam of a gridded ion source. The utility of these preliminary data and importance in the context of limited duration testing are discussed in Section V, and their extensibility to future development of test facilities are outlined in Section VI.

II. Experimental Setup

A. Halter Prototype

Colorado State University and University of Michigan are developing two configurations of the Halter system for initial prototype testing. Both rely on applied magnetic fields from either solenoids or permanent magnets to produce a magnetic field parallel to the isolated ion energy suppression plate surface. In this configuration the bias applied to the ion energy suppression plate creates an electric field perpendicular to the applied magnetic field and antiparallel to the incident beam ions as shown in Figure 2. The only surface exposed to ions with full beam energies are structures related to supporting the generation of the applied magnetic field (i.e. solenoid components or covers or permanent magnets). As stated previously, remotely located solenoids have the advantage of large transparency, decreasing the area of surfaces sputtered by full beam energy ions. A prototype of a solenoidal system was constructed, and the results are presented in the companion paper [16]. The configuration of the Halter studied herein relies on lines of permanent magnets that are placed facing one another (north to south) with the open area between them considered the open area through which ions will flow until they encounter the ion energy suppression plate, as shown on the right of Figure 1 – the "picket-fence" configuration. The magnets in the picket fence Halter system are used to apply the magnetic field parallel (transverse) to the surface of the ion energy suppression plate.

A prototype of this configuration was constructed for initial evaluation in the beam of an 8-cm ion source and is shown in Figure 3. The prototype consisted of 5 rows of magnets with 10 SmCo-26 magnets per row. The rows are spaced roughly 3.3-cm apart across an 18cm long and 20 cm wide area. The row length exposed to the beam was roughly 20 cm, and the grounded graphite strips protecting the magnets are 1.3 cm wide, which are removed in Figure 3 to show the magnets. The magnetic field of the open area between the lines of permanent magnets was mapped, with the magnitude of the field shown on the right in Figure 3. The resulting transparency of the active area Halter picket-fence prototype was roughly 0.73.

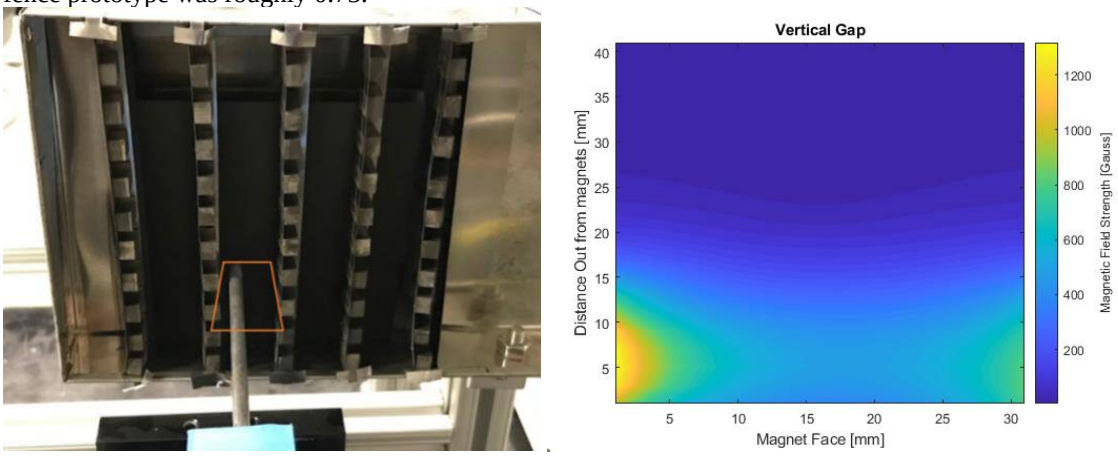

Figure 3: Photograph of the magnetic mapping setup (left) and resultant contour plot of magnetic field strength between two rows of magnets (right).

All exposed stainless steel and magnet rows were covered with thin graphite plates before testing of the Halter prototype in the beam of the ion source. The majority of the exposed region of the Halter to the ion beam was graphite apart from the stainless steel ground plate retainer brackets (shown at the ends of each row on the left of Figure 3). The temperature of the Halter prototype was not monitored, although post test measurement of the magnetic fields indicated no degradation of the permenent magnets was observed.

B. Gridded ion source test facility

An 8-cm gridded ion source was utilized in the Hydra vacuum facility at Colorado State University to evaluate the picket-fence Halter prototype. The Hydra facility has a pumping speed of 1000 L/s on argon (used in initial testing). The 8-cm gridded ion source utilized an additively manufactured titanium grid-set. The grid-set was printed with a concave dish for creating a focused, narrow-waisted ion beam at test locations of interest. The manufacture and initial evaluation of these grid-sets are detailed in [17]. The gridded ion source utilized a tungsten filament cathode for the discharge and a hollow cathode for the neutralizer. The ion source was operated on argon at the same flows – 4 sccm to the source and 2.5 sccm to the neutralizer – and at a beam current of 50 mA across all tests performed in the present study. Full Halter I-V curves were recorded at each of three axial locations as the beam voltage was adjusted from 200V to 600V in 100V increments. In addition, the Halter was translated in the z-direction while the floating voltage was measured for all of the gridded ion beam operating conditions.

A Faraday probe was utilized to map the ion current density in the regions of interest for Halter testing downstream of the ion source. The Faraday probe was translated on a two-dimensional motion stage to measure the axial current density from 110mm-410mm axial distance from the source exit plane, and -75mm to 80mm in the transverse (radial) direction relative to the ion beam centerline. A typical ion current density map is shown in Figure 4. The Halter prototype I-V measurements were made at three axial locations of 210mm, 310mm, and 410mm, which are shown in Figure 4 alongside a photograph of the Halter system under test at test position 1 (210 mm). The active area of the Halter prototype is large enough to contain the majority of the ion beam at all three test positions.

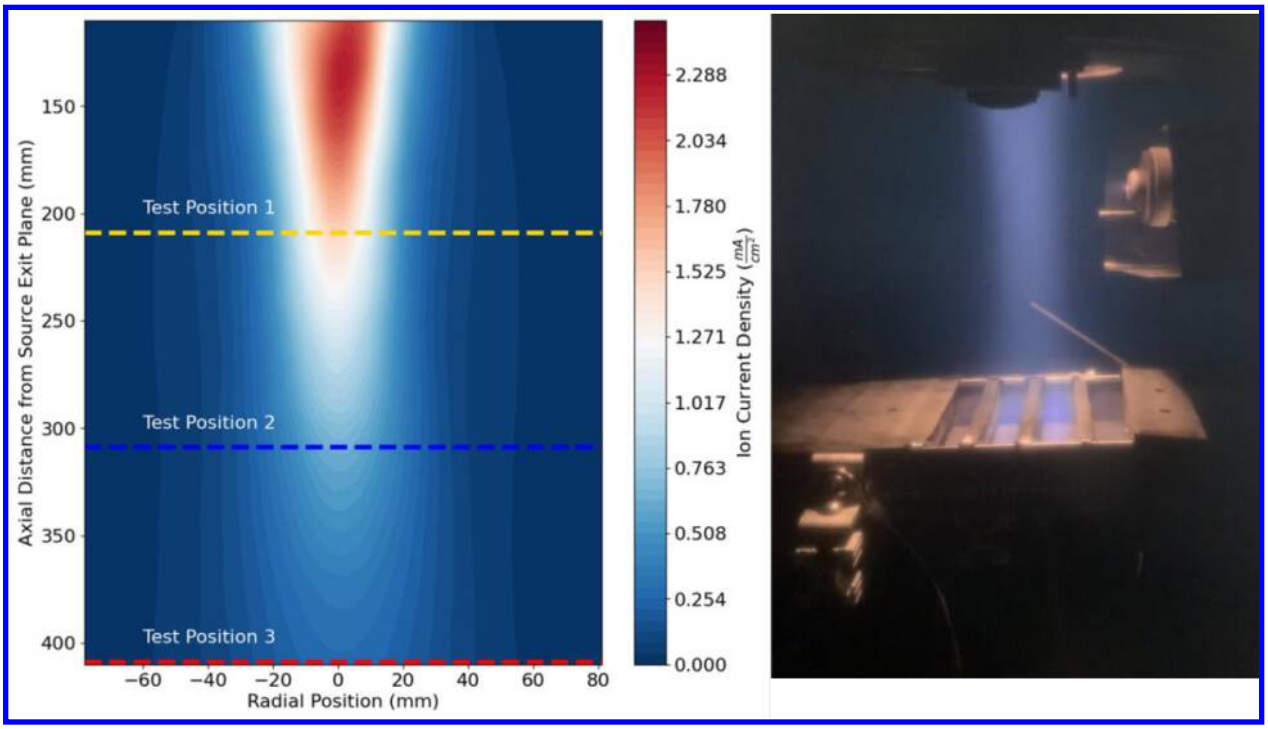

Figure 4: Ion current density measurements downstream of a converging ion beam gridset with annotated axial test locations for Halter prototype evaluation (left) and a photograph of the Halter under test at the closest 210mm test location (right).

III. Simplified Halter Model

A. Backsputter Model

The backsputter model is comprised of two sub-models, an ion plume and a sputter model. The ion plume model is used to provide the number of ions and charge-exchange-produced fast neutrals expected to arrive at the surface of a Halter system. The sputter model predicts the amount of backsputter material that will arrive back to a thruster or co-located quartz crystal microbalance (QCM) for the given ion and fast neutral energy and angle of incidence. The axial positioning of the Halter system at some location (z) and the relative geometry and features of the Halter system can be adjusted to accommodate several test conditions. For example, a representative 1m by 1m Halter prototype was used to predict the expected effectiveness, in terms of backsputter reduction relative to a grounded graphite plate, in the beam of a 1.5kW Hall thruster (presented in Section IV.B). The simulated quarter of the Halter system is shown in Figure 5 next to a photograph of the smaller Halter prototype evaluated downstream of a the 8-cm ion source. The quarter view of the 1m^2 system assumes a 2cm width of the ground plate and a 6cm spacing between the magnets, with the assumed ion energy suppression plate bias at 200V relative to ground.

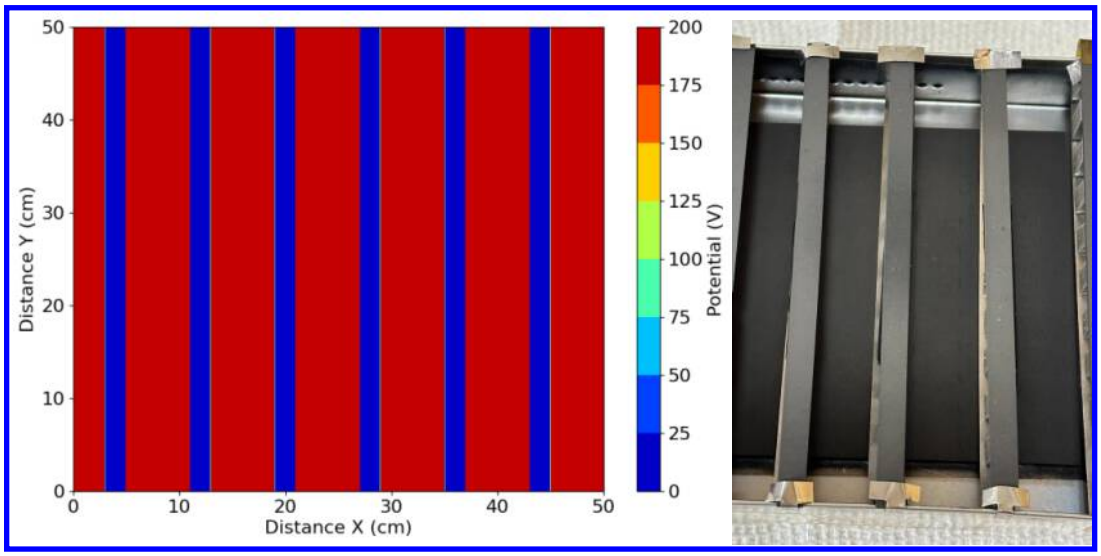

Figure 5: Quarter view of the potential profile of picket-fence magnetic configuration Halter system with a 200V bias applied to the ion energy suppression plate (left) and photograph of experimental prototype used in 8-cm gridded ion source testing (right).

1. Hall Thruster Plume Model

To assess the backsputter of facility material to a given thruster, it is necessary to quantify the total sputter-capable fluence to the Halter system surfaces. To do this, the current density data of a 1.5kW Hall thruster was fit to a two-term Gaussian, similar to that used by Pencil et al. [18]. The fit provides the current density with respect to radial distance, r, from the face of the thruster centerline and the angle from the thruster centerline, θ.

$$j(r,\theta) = \frac{R^2}{r^2}\left[k_0 \exp\left(-\frac{\sin\theta^2}{k_1^2}\right) + k_2 \exp\left(-\frac{\theta^2}{k_3^2}\right)\right] \quad (1)$$

Here the parameters k_0, k_1, k_2, and k_3 are fit to current density measurements made on an arc, at some R distance from the thruster. The current fraction of doubly ionized xenon or krypton atoms in the beam is left adjustable but is typically assumed to be 18-20%, which is representative of doubly charged ion current fractions measured in the plume of Hall thrusters [19]–[21]. The raw current density measurements are corrected for charge exchange according to equation (2) and use charge-exchange (CEX) cross-section fits from Miller et al. [22] and Hause et al. [23] for xenon and krypton, respectively.

$$j_{meas} = j_{beam} \exp(-\sigma_{CEX} n_0 z_{dist}) \quad (2)$$

The fraction of sputter-capable fluence that arrives at the Halter system as a neutral will be unaffected by the ion energy suppression biases, and therefore these particles will sputter with yields akin to surfaces that are unbiased. This

aspect of the model allows the examination of the effect of increased facility background pressure on the effectiveness of the Halter system. As the background pressure or axial spacing increases, the resultant fraction of sputter capable fluence that is neutral increases, and the effectiveness of the Halter diminishes as it cannot slow incoming fast neutrals.

2. Sputter Model

The sputter model relies on differential sputter yield estimates and solid angle calculations to predict the rate of back sputtered atoms to the thruster or co-located QCM. The size and axial distance of the Halter system from the thruster is used with the beam model to determine the sputter capable fluence energy and angle as well as the solid angle for each sputter location on the discretized Halter area. The solid angle for which the sputtered material will be ejected on a trajectory to deposit on the thruster or QCM is calculated across the simulated quarter plate area. Graphite is the primary material of interest as it is common practice to use this material for beam dumps and facility wall protection due to its low sputter yield. It is also the material used in the ground plates and ion energy suppression plate in the Halter system.

Previous models of backsputter utilized a cosine distribution to approximate the differential sputter yield for convenience and to negate the need for fitting free parameters from semi-empirical fits [3]. At higher ion energies, this is more accurate; however, under cosine behavior is often observed at lower energy ion sputtering, with strong variations in forward and backward sputter yield profiles as the angle of incidence is varied from normal sputtering [24], [25]. An example of the difference between cosine and under cosine behavior observed in differential yield sputter measurements is shown in Figure 6. taken from [25].

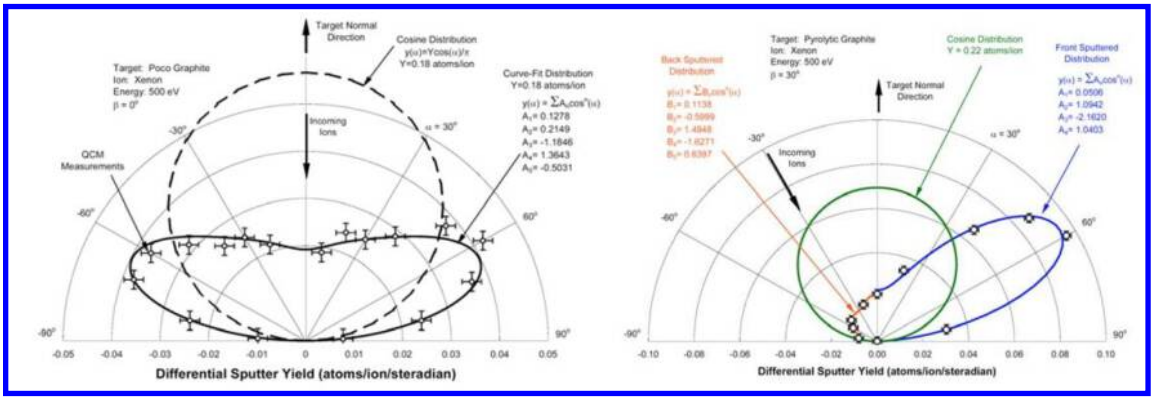

Figure 6: Differential sputter profiles measured on poco and pyrolytic graphite at normal (left) and off-normal (right) ion incidence compared to cosine distribution, taken from [25]**.**

A modified Zhang fit, developed by Yalin et al. [24] based on differential sputter yield fit work by Zhang & Zhang [26] was used to provide a continuous function for the differential sputter yield at each Halter operating condition explored. The modified Zhang fit can more accurately capture the under-cosine, as well as the forward and back sputter behavior observed, which may be critical as ions slowed by the Halter beam catcher are reduced to lower energy values.

The Hall thruster ion plume model provides the number, angle of incidence, and energy of the sputter capable fluence to the Halter system. The energy of the incoming ions is assumed to be near that of the anode voltage. If an ion is arriving at the ion energy suppression plate, it is assumed to be slowed by the magnitude of the potential difference between the ion energy suppression plate and ground, $\Delta E_{reduction} = q\left(V_{anode} - V_{ion\ supression\ plate}\right)$. Fast neutrals produced by CEX collisions are assumed to have no reduction in energy upon striking the ion energy suppression plate.

The modified Zhang expressions (3) and (4) provides the differential sputter yield at a given azimuthal (ϕ) and polar (α) angle as a function of bombarding ion energy E, angle of incidence β, and two free-fitting parameters, the total sputter yield $Y(E,\beta)$ and characteristic energy E^*. Efforts to model the carbon transport back to the thruster require the use of a continuous function that can provide the differential sputter yields at a given θ and ϕ as a function of the incident ion energy E, and angle of incidence β. To achieve this, the fitting parameters Y and E^* need to be cast in a

functional form that captures the behavior across a range of energies and angles of incidence. The differential yield from the modified Zhang is given by:

$$y_{MZ} = \frac{Y}{1-\sqrt{\frac{E^*}{E}}\cos(\beta)} \frac{\cos(\alpha)}{\pi} \left[1 - \frac{1}{4}\sqrt{\frac{E^*}{E}}\left(\cos(\beta)\,\gamma(\alpha) + \frac{3}{2}\pi\sin(\alpha)\cos(\phi)\right)\right] \quad (3)$$

and

$$\gamma(\alpha) = \frac{3\sin(\alpha)^2 - 1}{\sin(\alpha)^2} + \frac{\cos(\alpha)^2\,(3\sin(\alpha)^2 + 1)}{2\sin(\alpha)^3} \ln\left(\frac{1+\sin(\alpha)}{1-\sin(\alpha)}\right). \quad (4)$$

The relationship between the characteristic energy, E^*, and the angle of incidence β and the ion energy E was found to fit well to

$$\frac{E^*\cos(\beta)}{E_{th}} = C\left(\frac{E}{E_{th}}\right)^n \quad (5)$$

by Yalin et al. [24] for molybdenum targets, where the threshold energy E_{th} is assumed to be known and the constant C and n were free fitting parameters. For molybdenum, C and n were fit to 0.8 and 0.75, respectively. This leaves the total sputter yield, Y, as the only unknown for the modified Zhang. Total sputter yield has been shown to be well captured by energy dependent [14] and angularly dependent [27]models and were fit extensively for several materials including graphite by Yim in 2017 [15]. The Eckstein energy dependence sputter yield model includes E_{th}, needed to calculate characteristic energy, E^*, from (5), leaving the fit constants C and n as the only unknowns.

Ideally, we would utilize a similar Bayesian parameter estimation approach to fit the constants C and n for the existing graphite data provided by Williams' et al. [25], however, initial modeling efforts suggested a different form of relating E^* to E_{th} may be required. To obtain preliminary sputter results for purposes of evaluating the model, the same fit parameters for C and n, from [24] for Mo were utilized for graphite sputter data. Utilizing these fit parameters, the modified Zhang model qualitatively matches the profile of the differential measurements made by Williams et al. [25], and appears to be a much closer approximation for low energy yields than previous cosine-based approaches [3]. Total yield $Y(E,\beta)$ was provided from the best fit parameters for graphite from [15] using the Eckstein energy dependent and Wei angular dependent models. The differential sputter yield values $y(E,\beta,\theta)$ were provided by references (3)-(5). Figure 7 shows an example three-dimensional plot of the differential yield of graphite under 300eV xenon bombardment at 30 and 15 degrees of incidence.

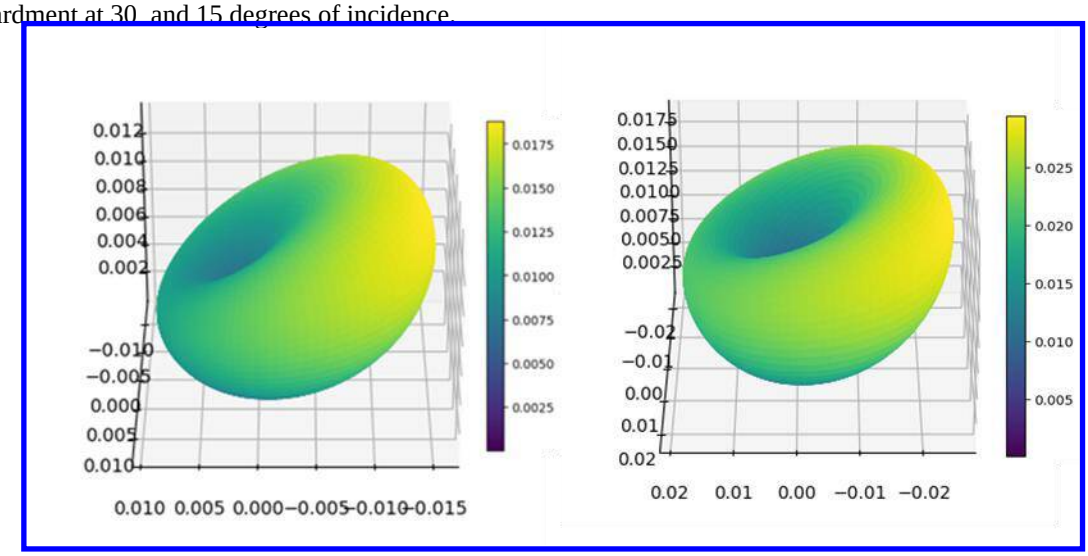

Figure 7: Example 3D plot of a modified Zhang differential sputter yield assuming ion energies of 300eV and an angle of incidence of 30 degrees (left) and 15 degrees (right).

Simulations of sputter capable fluence to a quarter model of a 1 m x 1 m picket fence halter placed 1 m downstream of a 1.5kW thruster beam operated at 300V is shown in Figure 8 utilizing the modified Zhang fit for graphite and the plume model fit to a 1.5kW a Hall thruster described in [28]. The left most contour plot shows the predicted sputter-capable fluence arriving at the Halter system, while the right most plot shows the predicted back sputter rate to the thruster face 1 meter away with an assumed ion energy suppression plate voltage of 200V.

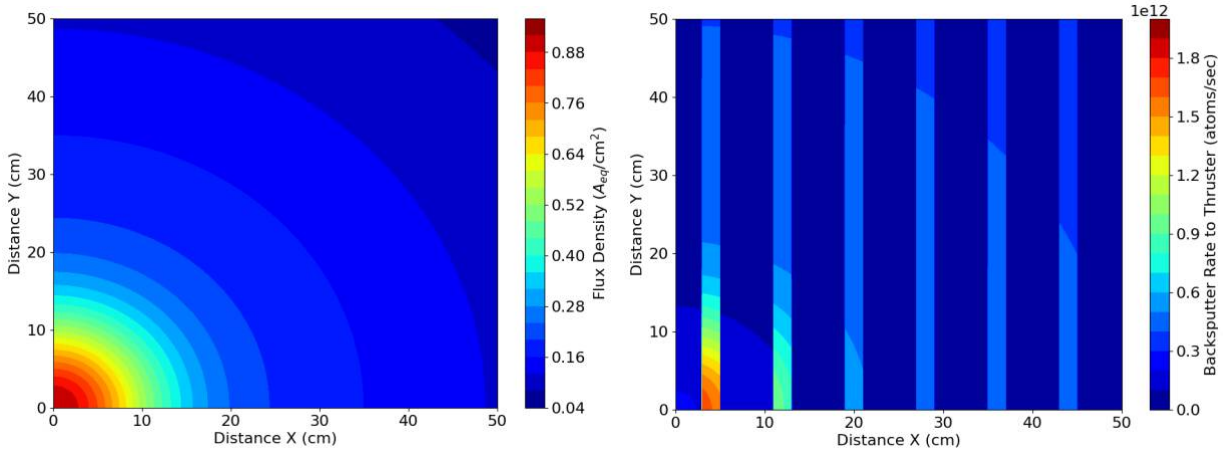

Figure 8: Left: Total fluence of ion and sputter-capable neutrals arriving at a 1m x 1m Halter system placed 1.5m downstream of a 1.5 kW HT operated at 300 V. Right: Simulated backsputter of graphite from the Halter system with the ion energy suppression plate assumed to be a 200V.

The primary purpose of the backsputter model is to predict how well a given system might be able to reduce the back sputter to a thruster. In the results presented in this paper the relative decreases in backsputter rate are compared to that of a grounded graphite plate of the same size in the same location relative to the thruster. Sputtering of facility wall and other surfaces are not currently included in the model.

B. Halter Current-Voltage Model

A model of the current collected at the Halter ion energy suppression plate as a function of applied bias to the plate was developed to gain an understanding of how Halter design choices affect the system's performance under different beam plasma conditions. This was done to gain a broader understanding of the device and obtain insight into how the system could be improved. The general outline of the model is described herein, with results presented in Sec. IV.C, and discussion of limitations in Sec. V.

The model relates properties at the sheath edge near the plate, denoted s, to the incoming plasma properties, denoted p, at the upstream entrance of the Halter plate. Both the ion and electron current to the plate are evaluated at each applied ion energy suppression plate bias V, which is referred to as the sheath voltage in the model, to predict the net current to the plate of the Halter system. The electron current to the plate can be characterized using a generalized Ohm's law approach with the electron current density written as

$$j_e = E\frac{q^2 n_e}{m_e}\frac{\nu_c}{\omega_e^2 + \nu_c^2} \quad , \tag{6}$$

where E is the electric field in front of the ion energy suppression plate, q is the fundamental charge, n_e is the electron density in the plume in front of the Halter system, m_e is the mass of an electron, ν_c is the classical collision frequency (that could be replaced with a term that could include anomalous collisions), and ω_e is the gyrofrequency of the electrons. The electric field is assumed to be linear across the Halter magnetic sector $E = V/L$, where L is the length of the magnetic section that ions and electrons must travel across to arrive to the plate.

The ion current density is captured by taking the first moment of the ion velocity distribution

$$j_i = qn_e \int_0^\infty v_s \, f_i \, (v_s)|_s dv_s \quad , \tag{7}$$

where v_s is the velocity of the ions near the sheath edge. This velocity can be related to the incoming velocity of plume ions by applying conservation of energy to derive the characteristic equation

$$v_s = \sqrt{\frac{2q}{m_i}\left(V_p - V_s\right) + v_p^2} \quad , \tag{8}$$

where V_p is the plasma potential and V_s is the sheath potential. The change in the ion energy distribution is characterized by the one-dimensional steady-state Vlasov equation

$$v\frac{\partial f_i}{\partial x} = -\frac{qE}{m_i}\frac{\partial f_i}{\partial v} \tag{9}$$

that can be used to relate the incoming velocity distribution to that at the sheath edge. This solution results in an ion current that is related to the incoming ion energy distribution and potential difference between the sheath and the plasma potential through

$$j_i = qn_e \int_{V_s - V_p}^\infty v_p \, f_i \left(v_p \rightarrow \, E_p\right)\big|_p \, dE_p \quad , \tag{10}$$

where the ion velocity distribution $f_i \left(\mathrm{v_p}\right)|_p$ is evaluated at the plasma plume. The incoming ion energy distribution is assumed to be a low temperature, $T_{ion} = 0.5\ eV$, Maxwellian distribution drifting at the beam speed u_b represented as:

$$f_i(v) = \left(\frac{m_i}{2\pi \, q \, T_i}\right)^{1/2} e^{-\frac{m_i (v-u_b)^2}{2q\,T_i}} \quad , \tag{11}$$

where m_i is the mass of the ion, T_i is the ion temperature, and q is the fundamental charge. This velocity distribution can be related to the ion energy distribution through

$$f_i\left(E_p\right) = \left(\frac{m_i}{2\pi \, q \, T_i}\right)^{1/2} e^{-\frac{m_i\left(\sqrt{\frac{2\,q\,E_p}{m_i}} - u_b\right)^2}{2q\,T_i}} \quad , \tag{12}$$

with E_p representing a specific ion's energy prior to entering the Halter system. The ion current density at the plume edge of the device is considered a measured quantity j_i. The ion current density that arrives to the plate is characterized by the fraction of the plume ions that have sufficient energy to overcome the difference between the sheath voltage V_s and the plasma potential V_p.

Now with equations that relate both ion current density and electron current to sheath voltage and plasma potential, we can write an expression for the total current to the plate as

$$I = A\,(j_e + j_i) = Aqn_e\left[E\,\frac{q}{m_e}\frac{\nu_c}{\omega_e^2 + \nu_c^2} + \int_{V_s - V_p}^\infty f_i \left(v_p \rightarrow \, E_p\right)|_p dE_p\right] \tag{13}$$

Initially only classic collisions are considered through

$$\nu_c = 2.9 \times 10^{-12} \, \frac{\ln \Lambda \, \langle n_e \rangle}{(T_e)^{3/2}} \tag{14}$$

where the Coulomb logarithm, $\ln \Lambda$, is given by

$$\ln \Lambda = 23 - \frac{1}{2}\ln\left(\frac{10^{-6}\langle n_e \rangle}{(T_e)^{\frac{3}{2}}}\right) \tag{15}$$

and where $\langle n_e \rangle$ is the averaged plasma density in the magnetic sector of the plate. Here we assume the average density is the mean of the sheath and plume density $\langle n_e \rangle = \frac{n_e + n_s}{2}$, where n_s is given by

$$n_s = n_e \int_0^{\infty} f_i \left(\sqrt{\frac{2q}{m_i}(V_p - V_s) + v_p^2} \right) \Big|_p dv_p \tag{16}$$

If we assume that the Hall parameter is significantly large, the plasma potential V_p is near 0V, and that the sheath potential V_s is negligible to that of the ion energy suppression plate bias V_s, (13) can be rewritten as

$$I = A\,(j_e + j_i) = Aqn_e \left[-\frac{V}{L}\frac{q}{m_e}\frac{\Gamma}{\omega_e^2}\ \frac{n_e}{2\,(T_e)^{3/2}} \left[\int_0^{\infty} f_i \left(\sqrt{v_p^2 - \frac{2q}{m_i}V} \right) \Big|_p dv_p + 1 \right] + \int_V^{\infty} f_i\,(v_p \rightarrow E_p)\big|_p dE_p \right]. \tag{17}$$

This equation for total current to the plate was fit to measurements presented in the next section. Details of experimental parameters and fit modification are detailed in Section IV.C.

IV. Results

A. Initial Experimental Results – Picket-Fence Configuration in a Gridded Ion Source Beam

The prototype picket-fence configuration of the Halter system was evaluated in the beam of the 8-cm ion source described in Sec. II.B. The Halter was mounted to a motion stage, which was used to set the axial location between the source and the Halter at 210mm, 310mm, and 410mm for detailed evaluations. The current density was mapped across this region with a Faraday probe mounted to a 2D motion stage able to discreetly sweep across several axial and radial locations centered on the gridset centerline. The resulting current density map is shown in Figure 4. The ion source was operated at the same beam current for each test, while the beam voltage was varied.

At each location the current to the ion energy suppression plate with respect to the applied plate voltage (referred to as the I/V curve) was measured as the ion source was operated at beam voltages from 200V to 600V. The applied bias voltage was swept 100V past the beam voltage in all tests except the 600V operating condition due to power supply limitations. The current measurement convention we use is similar to that of an RPA, with positive current representing ions arriving at the plate, and negative current indicating net electron current to the plate. The resultant I/V curves for the 210mm and 310mm test locations are shown in Figure 9. A fair amount of curve overlap is present in the closest test location with the majority of the curves crossing the zero net current point – the floating voltage – within 50V of each other. The relatively steep slope of the curves indicate that there is significant electron transport to the plate even at low voltages as there is no distinct 'knee' in the curve that would traditionally represent the ion energy distribution expected from an ion beam source. In the second test location, 310mm, the lower beam voltage I/V curves begin to separate out with more easily distinguishable floating voltages especially for the lower beam voltages that were evaluated. In these plots there is a relatively significant drop in current, indicating decreased ion current, at voltages around 80% of the beam voltage.

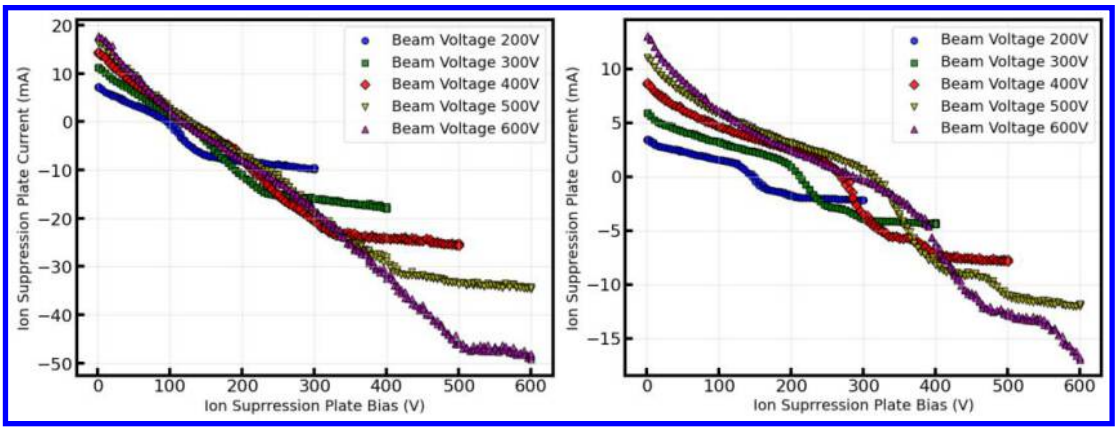

Figure 9: Ion energy suppression plate current with respect to applied bias for the 210mm (left) and 310mm (right) test locations.

The current collection curves at the 410 mm test location, shown in Figure 10, continue the trend of spreading out the I-V traces with beam voltage conditions. Furthermore, the inflections contained in each curve, represented by the local maxima of the slope $-\frac{dI}{dV}$, indicate two distinct ion groups, annotated with ovals in Figure 10. Another distinct feature of the collected currents is the saturation observed at biases above the beam voltage for all test conditions, except 600V as it was not swept to sufficiently high biases to observe saturation.

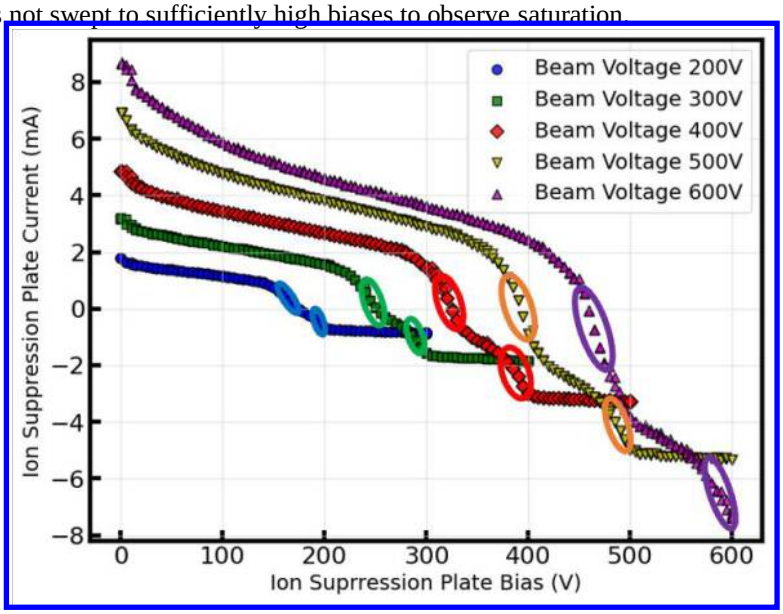

Figure 10: Ion energy suppression plate current with respect to applied bias at 410mm axial distance from the gridded ion source.

If the Halter ion energy suppression plate can achieve floating voltages sufficiently high to reduce sputtering, then no power would be required to operate the system and minimal perturbations will be imposed on the thruster (due to equal numbers of ions and electrons being collected). Furthermore, no ion-induced secondary electrons would be released by the Halter like they are from traditional beam targets, which would further reduce thruster-facility interactions. As noted in the I/V curves presented in Figure 9 and Figure 10, it was observed that the floating voltage was increased as the Halter system was moved further downstream of the ion source. To investigate this trend in more detail, the ion energy suppression plate floating voltage was measured while the Halter system was moved from 210-410mm downstream of the source. The resulting floating voltage profiles for each beam voltage are shown in Figure 11. A clear trend towards saturation was observed as the Halter was positioned beyond 320 mm in regions that would be in the far field (greater than 4 ion source diameters downstream, however, in the near field ($z < 320$ mm) significant electron transport occurs thereby limiting the floating voltage.

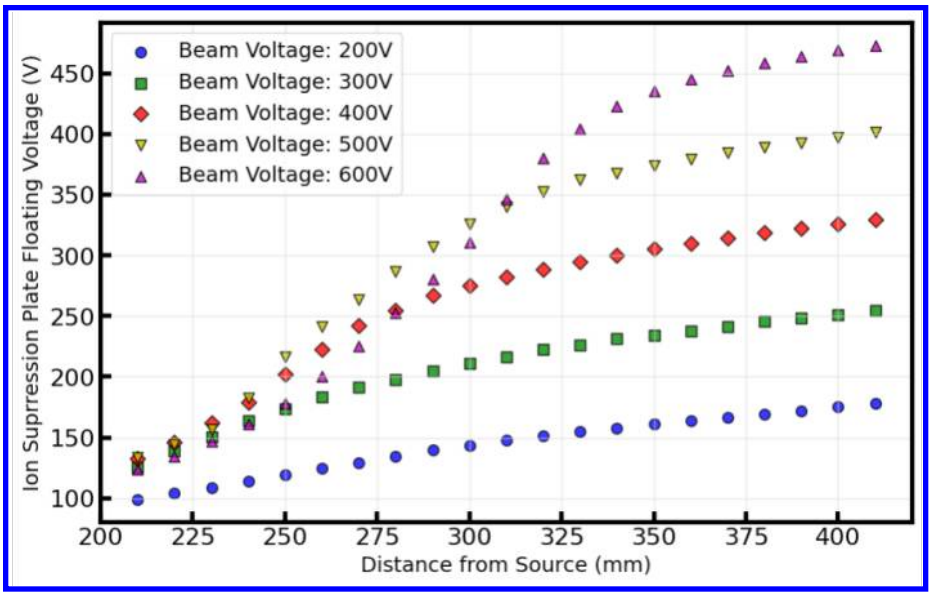

Figure 11: Floating voltage of the Halter ion energy suppression plate with respect to axial location downstream of the ion source.

A limited backsputter test was conducted utilizing a quartz crystal microbalance (QCM) mounted near the ion source. The QCM was monitored with an IMM-200 deposition rate monitor to evaluate relative changes to the backsputter rate as the ion energy suppression plate was varied. Figure 12 shows how the backsputter rate changed with applied bias relative to the observed rate with a 0V bias applied at the 310mm location. The uncertainty in the measurement is based on the repeatability of the 0V bias condition across the length of the test. The QCM was water cooled and allowed to reach thermal equilibrium at each condition before changing biases. A thermocouple connected to the QCM had failed and was therefore unable to indicate temperature at the suppression plate biases that were evaluated. No drift in deposition rate was observed from the initial step change that occurred at a given suppression plate bias. It is important to note the QCM measurement indicated net erosion at the 600V condition and a higher than expected change at 500V, which could indicate that ions were being reflected back toward the QCM from the Halter or that ions were being formed within the Halter and then accelerated from it toward the QCM.

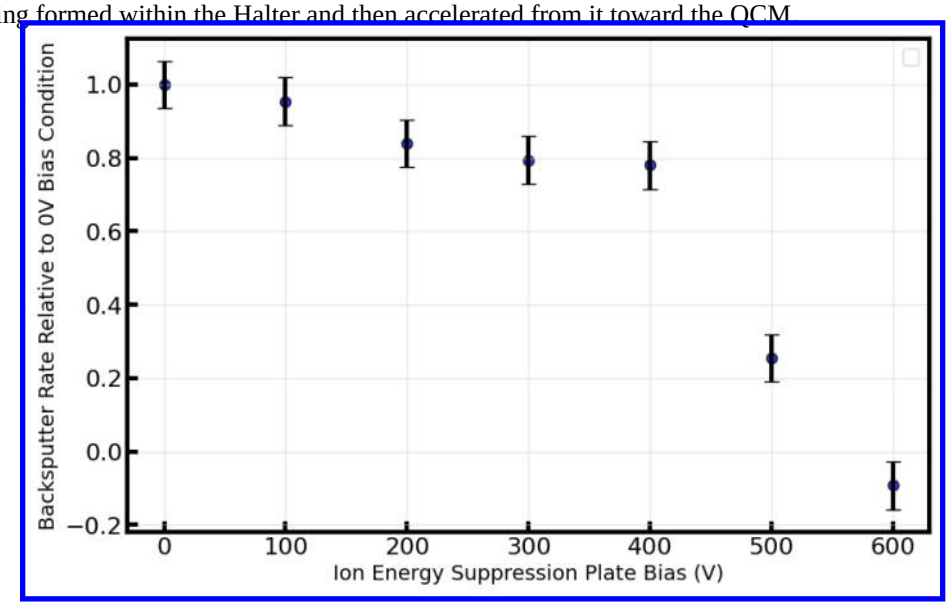

Figure 12: Relative changes to the backsputter rate as the Halter ion energy suppression plate bias was increased at during operation at a 600V ion beam operating condition.

B. Backsputter Model Results

The backsputter model was leveraged to determine the expected effectiveness of different Halter configurations and thruster operating conditions. The two primary features of interest to evaluate were the effects of pressure on the system effectiveness and the impact of reduced open area fractions. To do this, the plume model from Sec. III.A.1 was fit to a representative current density profile of a 1.5kW Hall thruster tested at CSU. The sputter model from Sec. III.A.2 was then applied to the specified Halter configuration. For all model results presented herein, the Halter system was assumed to be 1.5m away from the thruster face and was assumed to be 1m by 1m with the center of the plate aligned with the thruster centerline, as shown in Figure 5. In each test, the thruster was assumed to operate in two different anode voltages, 300V and 600V, respectively.

In evaluating pressure effects on Halter operation, the ion energy suppression plate was assumed to be 80% of the anode voltage, which floating voltage measurements of the prototype from Figure 11 indicate is possible. Calculations for the backsputter rate were repeated for a range of pressures from 10^{-6} Torr to 10^{-4} Torr. As pressure increases, the fraction of the sputter-capable fluence arriving at the Halter system as neutrals (with assumed beam velocities) will increase. This increase in fast-moving neutrals arriving at the Halter will, in turn, reduce the overall system effectiveness as neutral species are unresponsive to the applied electrostatic fields. This effect is shown clearly in Figure 13 as the backsputter rate increases from around 30% relative to a grounded graphite plate at low pressures up to nearly no reduction at 1E-4 Torr.

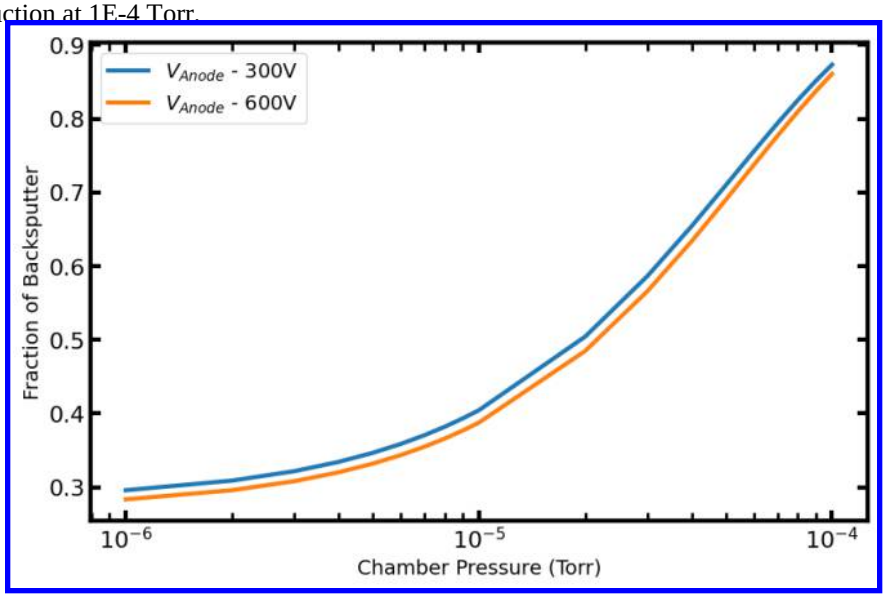

Figure 13: The simulated effect of background pressure on backsputter reduction of the Halter system compared to a grounded graphite plate with no magnetic field.

Another important feature to explore is the effect that open area fraction has on the Halter system. The open area fraction can largely influence the strength of the magnetic field as spacing between magnets or solenoid structures often limits achievable field strength for a given magnet strength or solenoid size. Sufficient magnetic field strength is required to avoid plume interactions that could affect test fidelity. The solenoidal configuration of the Halter may allow the suspension of a plate behind the transverse magnetic field with few if any, grounded surfaces in the path of the beam ions. Figure 14 shows the expected effectiveness of the Halter system utilizing scaled picket-fence and solenoidal configurations, with open area fractions of ~75% and 100%, respectively. Although the plate manages to capture the majority of the ion beam current, the achievable effectiveness is still limited by the presence of fast neutrals produced by CEX collisions at finite background pressures assumed to be 1E-5 Torr for the results presented in Figure 14.

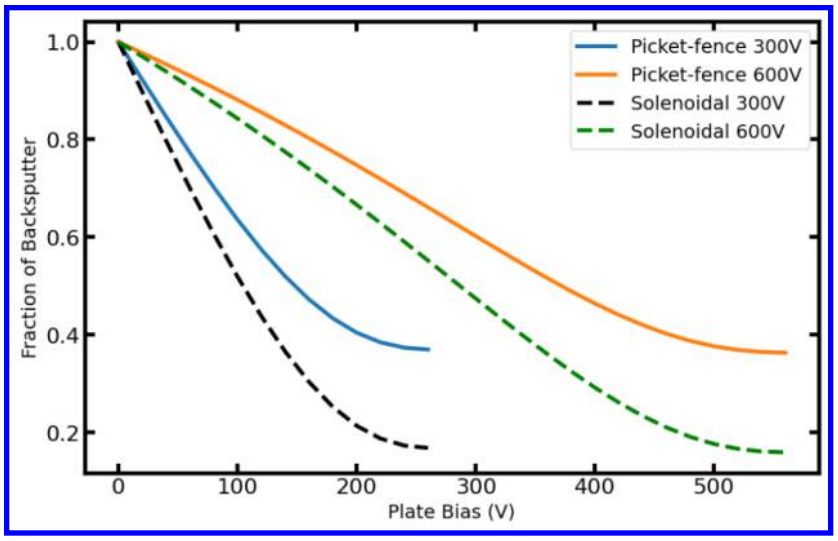

Figure 14: Simulated fraction of backsputtered material at two operating voltages with respect to the applied ion energy suppression plate bias relative to a grounded graphite plate with no magnetic field.

C. Halter Current-Voltage Characteristic Model

The current-voltage model of the Halter, described in Sec. III.B was fit to I/V curve measurements of the prototype picket-fence Halter configuration tested in the beam of an 8-cm gridded ion source. Parameters of the model can then be adjusted to observe how changes in beam conditions or magnetic field strength might affect Halter performance. Parameters of the model that were used as inputs were length L of the transverse magnetic sector, assumed to be ~8mm, and the average magnetic field strength B which was assumed to be near 450 G across weakest section between magnets. The incoming beam ion current density was taken from the current density mapping shown in Figure 4, with slight adjustments made for each beam voltage condition to achieve ion current agreement at the 0V bias condition. The area used in the model for ion current collection was adjusted to account for beam spreading observed in the current density mapping as axial distance was increased. However, due to the two groups of ions observed in Figure 10, the energy of the beam ions was allowed to be a free fitting parameter.

Early fitting of the model to measurements indicated that a larger electron current than permissible by the standard collision frequency, ν_c, was also required to fit the model to the data. As a result, an additional collisional term ν_α was added to ν_c to increase electron currents. Figure 15Figure 15Figure 15-Figure 18 show model predictions and measurements once the collision frequency was adjusted. This is discussed in further detail in Section V. Figure 15 shows the best fits of the model to each of the experimentally captured I/V curves at the 410 mm axial location. The lower beam voltage conditions appear to fit better to the model while more disagreement is present between the model and higher voltage measurements. However, it is worth noting that the 600V condition did not contain plate biases above the beam voltage due to power supply limitations, which would have likely improved the fit results for the 600V beam condition.

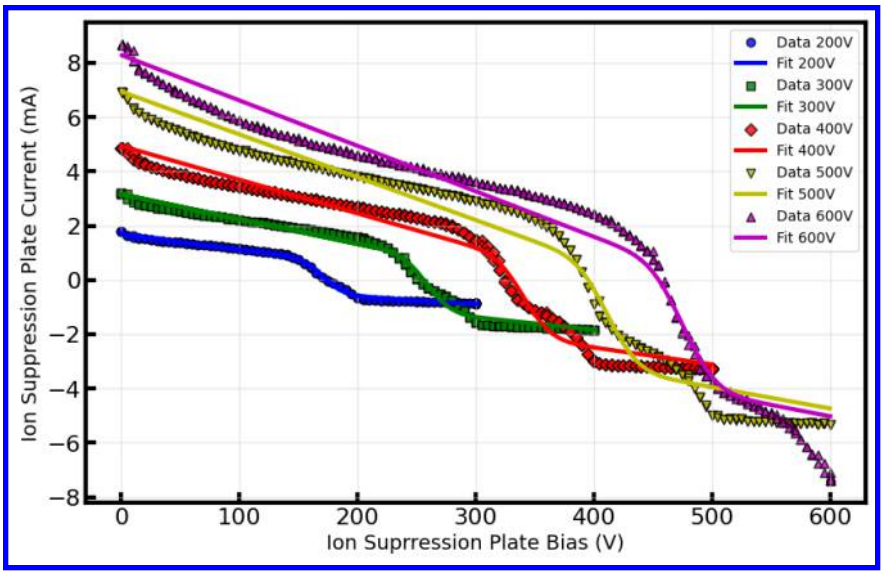

Figure 15: Fit of the current-voltage model to the experimentally collected I/V curves collected 410mm away from the 8-cm ion source.

The 200V beam condition had the best fit and was therefore used to evaluate the effect of adjusting parameters of interest such as magnetic field strength and ion current density. Figure 16 shows the fit to the 200V condition but with examples of what the model predicts would happen with better and worse confinement of electrons by the magnetic field by adjusting magnetic field strength. In this comparison, the ν_α term was assumed to remain unchanged for each trace, although we note that this is likely not the expected behavior. The strong B-field curve is representative of a scenario similar to an ideal retarding potential analyzer (RPA) where net ion current is collected with no electron current until sufficient voltage is achieved to repel all ions. This would be the ideal I/V curve behavior of the Halter. The weakly magnetized electron case (low B-field) resembles that of the data collected closer to the ion source at the 210mm and 310mm test locations.

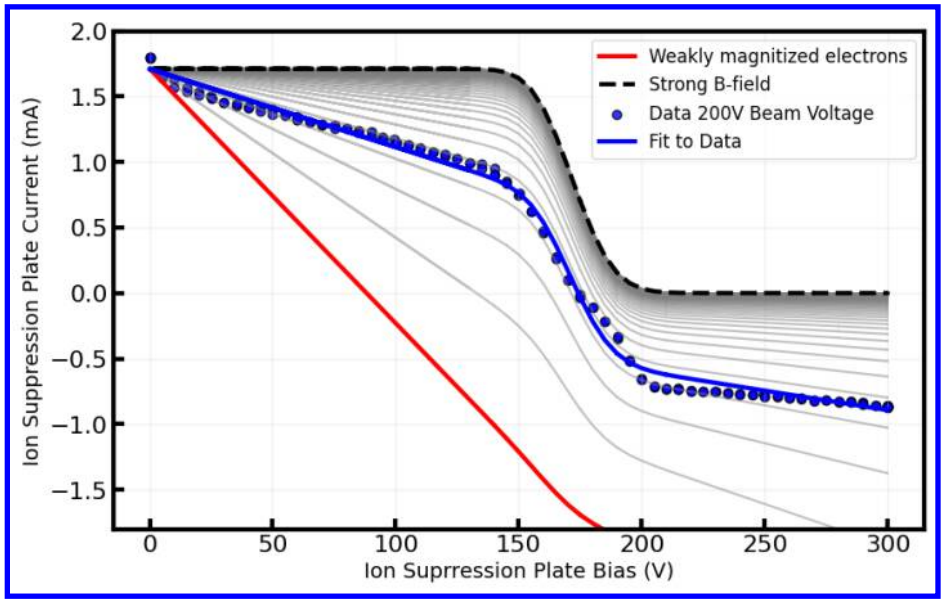

Figure 16: Evaluation of the current-voltage model fit to the 200V beam voltage I/V trace collected at the 410mm location with reference curves representing weaker and stronger magnetic fields.

The model had a difficult time fitting to the experimentally collected I/V curves at the closer locations if the B-field was forced to remain near the measured values even with significant ν_α values, however, if weaker B-field values were permitted, by an order of magnitude, then the general shape of the I/V curves could be qualitatively fit by the model. Figure 17 shows the fits to these curves. This result is unexplained at the current time, and we plan to look into this issue in future work.

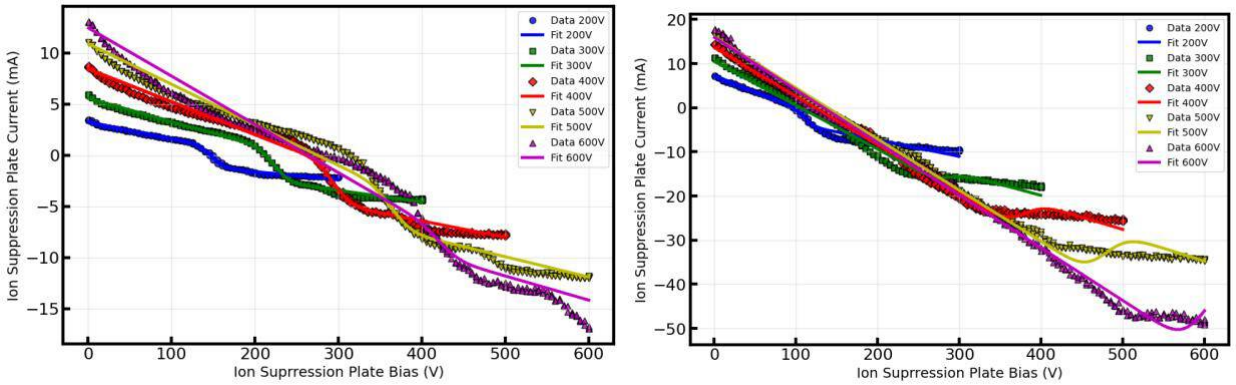

Figure 17: Fits of the current-voltage model to the 310 mm (left) and 210 mm (right) experimentally collected I/V curves, with weaker B-fields allowed.

The model can also allow us to examine the effects of increased ion current density at the Halter plate, as use in high-power testing will likely result in dramatically increased ion current densities. Figure 18 shows a similar fit to the 200V data at the 410 mm downstream location, with lines fit at ion current densities ranging from 20% to 500% of the measured ion current density, assuming no other changes. It is noted that no changes were made to the measured Halter B-field for the model results shown in Figure 18 like what was done to create Figure 17, and a normalized current density scale was used to better compare these trends. Figure 18 shows a clear reduction in the floating voltage as ion current densities are increased.

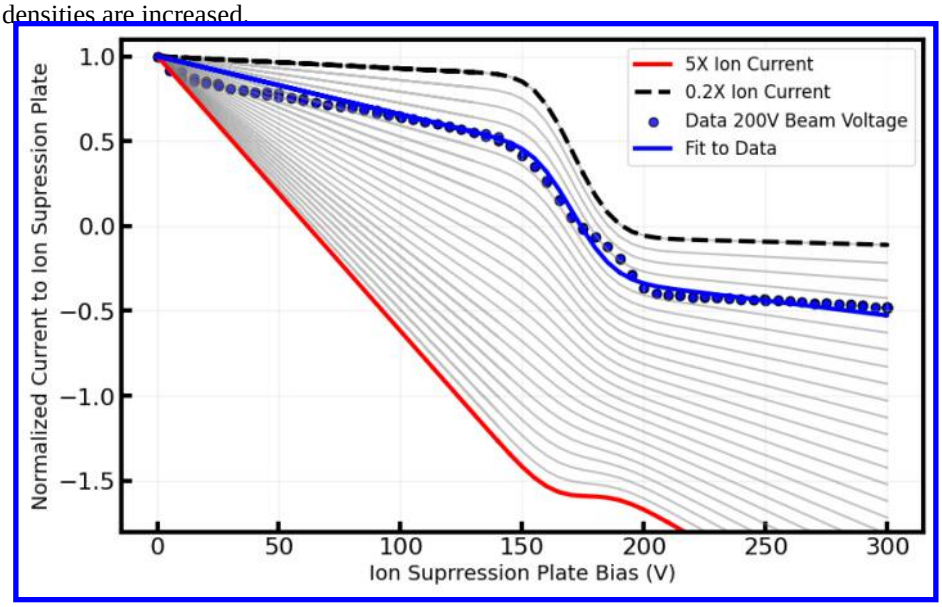

Figure 18: Model results for varied ion current density to the Halter compared to the 200V beam voltage fit.

V. Discussion

The initial modeling and experimental results of the Halter have yielded important insights into the design and implementation of the Halter beam catcher concept as a backsputter mitigation system. Here we discuss these insights and outline obstacles to future development of a backsputter mitigation system. Insight from evaluation of a prototype picket-fence configuration of the Halter and the sputter and current-voltage models are discussed in the context of how best to implement this concept at larger scales.

In the initial evaluation of the picket-fence Halter prototype in the beam of an 8-cm ion source, clear trends in the current traces and floating voltage sweeps indicated that further distances from the source lead to improved floating voltages—which is the primary figure of merit of the concept. At the 410 mm location, the floating potential was found to be nearly 80% that of the beam voltage, which is more than sufficient to reduce backsputter. The Halter current-voltage model also predicted a similar trend, where increased ion current density is expected to lead to poorer confinement of electrons. In the context of ground testing at low to moderate power levels, we believe that ion current densities equal to and lower than those measured at 410 mm are created in large test facilities at locations closer to the thruster than conventional beam targets are located. However, higher current densities are expected in high-power tests, which will require changes to the Halter design. One potential way to address this challenge would be to increase how well we can restrict electron current from high plasma density beam plasmas. While adjusting the bias of the buried plate to high potentials may reduce backsputter to some extent, biasing a plate in such a way with high electron current collection will perturb the thruster plasma plume and may cause the plasma potential and cathode floating potential to rise, thereby limiting effectiveness but also test fidelity [13].

In attempting to model the current to the Halter ion energy suppression plate, it was clear that significant electron transport is required to fit the measured current for a given plate voltage. An effective enhanced collision frequency ν_α was added to ν_c in the numerator of equation (6). Adding this free-fitting parameter allowed the modeled electron current to be increased sufficiently to match the measured data, and is likely representative of several factors. Increased collisions due to neutrals confined in the channel of the prototype, ion- and electron-induced electron emission from the grounded magnets that are in direct contact with the plasma, and anomalous electron transport are potential mechanisms for increasing electron current back at the ion energy suppression plate. It will be critical to evaluate the primary source of this increased electron current to the plate to implement design changes that enable better electron confinement, especially at increased current density regimes expected in high power (>20kW) testing. Ideally, increased magnetic field strength could enhance confinements as exemplified in Figure 16, but, if other losses continue to increase, then the expected improvements in confinement may not be realized. If net electron current is sourced from the beam plasma, then local plume plasma potential changes are expected. Future tests can implement diagnostics such as emissive probes in the regions directly upstream of the Halter system to evaluate if changes are observed during operation when net electron current is occurring.

On the point of test fidelity, the prototype picket-fence Halter system appeared to show two distinct ion current populations, as shown in Figure 10. The negative derivative of the plate current was taken with respect to applied voltage $-\frac{dI}{dV}$, as is done with retarding potential analyzers, is plotted against plate voltage in Figure 19. This would represent the ion energy distribution function for an RPA probe. We believe the double peaks observed at each beam voltage condition in indicative of two distinct ion populations that are eventually repelled by the bias applied to the Halter plate. These ions could be produced at two distinct potentials somewhere upstream of the Halter plate. The origin of the lower energy group of ions is still unclear, although we believe it may be a feature of a large amount of charge exchange observed within or near the Halter. It is important to understand how the ion-beam and Halter interaction might be causing the lower energy group and ensure that this is minimized when the system is scaled to larger sizes.

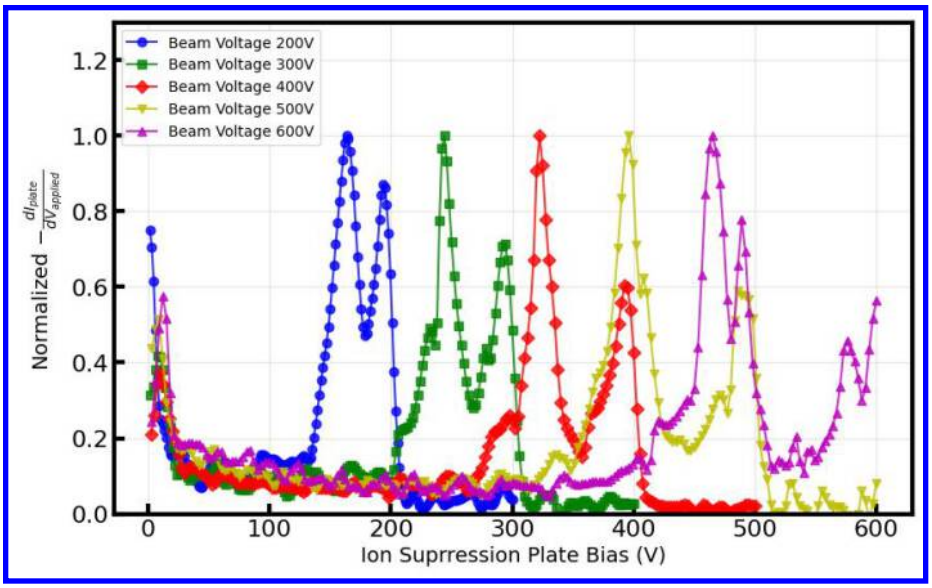

Figure 19: The normalized negative derivative of the ion energy suppression plate current with respect to applied voltage $-\frac{dI}{dV}$, plotted against the applied ion energy suppression plate bias.

A major goal of backsputter mitigation is to limit the masking of thruster erosion rates in higher power electric propulsion systems. In the brief QCM test used to evaluate backsputter reduction, when the ion suppression plate was biased near the beam voltage net erosion was measured at the QCM. Although not confirmed, we suspect that this is due to bombardment from charge exchange ions produced near the Halter ion energy suppression plate while held at elevated biases. These charge exchange ions that are unmagnetized can then be accelerated by the Halter's electric field to the lower potential regions in the plume, effectively sending high energy ions back at the thruster. This can be confirmed with an RPA or ESA placed near the ion source with the probes directed toward the Halter. We believe that the limited pumping speed of the small test facility and the large channel volume of the initial picket-fence prototype likely led to significantly high neutral gas pressures near the plate for sufficient charge exchange collisions to occur at these higher potentials. This can be mitigated by placing the Halter system sufficiently downstream and lowering the total volume of the system channels, in the picket-fence configuration of the system. Additionally, an segmented and open ion energy suppression plate design like that shown in Figure 1, can limit neutral trapping near the region of high positive potential.

Finally, it is important to note that the system will only be effective under a given pressure value. Although it is expected that the beam currents and backsputter rates will continue to increase with device power, complementary steps will need to be taken to mitigate large increases in background pressure that would limit the overall effectiveness of the Halter system.

VI. Conclusion

We presented an initial concept for reducing backsputter to electric propulsion thrusters by slowing down beam ions referred to as a "beam-catcher". We presented in further detail a specific form of the beam-catcher referred to as the "**Hall** **t**hruste**r** in **r**everse" or Halter that utilizes transverse magnetic fields to the surface a positively biased plate downstream of an electric propulsion device with the goal of slowing incoming beam ions to the plate. The slowing of ions aims to reduce the sputter of material by beam ions that is subsequently deposited back on the thruster. To evaluate the effectiveness of such a system, sputter and current-voltage models of the system were developed to better understand how design and operating conditions of the devices may affect performance. A prototype of the picket-fence configuration Halter system was tested in the beam of an 8-cm ion source to compare to initial sputter and current-voltage models, as well as key limitations of implementation.

Both the prototype test results and the current-voltage model indicate the Halter floating voltage will be reduced in high ion current densities due to large electron currents. With the aim of minimizing the impact to thruster operation

and maximizing achievable sputter reduction, operating the Halter with a floating voltage of ~80% of the beam voltage, or anode voltage in thruster testing, is likely a reasonable target if placed sufficiently far from the thruster. The sputter modeling indicated a significant reduction in Halter system effectiveness at higher operating pressures. Furthermore, we believe that charge exchange in regions near the ion energy suppression plate at sufficiently high biases resulted in the generation of high-energy ions directed back at the thruster, as indicated by net erosion observed with the QCM. Finally, the use of induced magnetic fields may increase system transparency, thereby increasing effectiveness over the picket-fence configuration.

Further testing and modeling are needed to confirm the effectiveness of the beam-catcher concept and, in particular, the Halter system. First, testing at larger thruster scales >50W ion thruster tested here will be important in confirming the observed trends. Prototype tests will also need to include more rigorous measurements of the plume characteristics to ensure little to no perturbation of the plume can be achieved during testing. Further development of the current-voltage and sputter models will help alleviate the need to test small design and operational changes before implementation at scales required of large test facilities used in high-power EP testing. This includes the extension of sputter modeling to include different chamber configurations, as it has been noted that in large length-to-diameter (L/D) vacuum facilities the Halter placement will be critical in ensuring that chamber side-wall contributions to backsputter do not dominate. Further treatment of the electron current to the Halter plate should be evaluated, as depending on the source of these electrons, reduced electron confinement may limit the effectiveness of the Halter system at higher ion current densities, and electrons sourced from the plume are expected to affect plume fidelity.

VII. Acknowledgements

This work was supported by the Joint Advanced Propulsion Institute, a NASA Space Technology Research Institute. (Grant: 80NSSC21K1118.)

References

[1] J. D. Frieman *et al.*, "Long duration wear test of the NASA HERMeS Hall thruster," in *2018 Joint Propulsion Conference*, 2018, p. 4645.

[2] J. D. Frieman *et al.*, "Wear test of the 12.5-kW advanced electric propulsion system engineering test unit Hall thruster," in *AIAA Propulsion and Energy 2020 Forum*, 2020, p. 3625.

[3] J. H. Gilland, G. Williams, J. M. Burt, and J. Yim, "Carbon Back Sputter Modeling for Hall Thruster Testing," in *52nd AIAA/SAE/ASEE Joint Propulsion Conference*, 2016, p. 4941.

[4] R. B. Lobbia, J. E. Polk, R. R. Hofer, V. H. Chaplin, and B. Jorns, "Accelerating 23,000 hours of ground test backsputtered carbon on a magnetically shielded Hall thruster," in *AIAA Propulsion and Energy 2019 Forum*, 2019, p. 3898.

[5] L. L. Su *et al.*, "Operation and Performance of a Magnetically Shielded Hall Thruster at Ultrahigh Current Densities on Xenon and Krypton," in *AIAA SCITECH 2023 Forum*, 2023, p. 0842.

[6] S. J. Hall *et al.*, "Performance and high-speed characterization of a 100-kW nested Hall thruster," *J Propuls Power*, vol. 38, no. 1, pp. 40–50, 2022.

[7] M. L. R. Walker *et al.*, "Overview of the Joint AdvaNced PropUlsion InStitute (JANUS)," 2022.

[8] E. Hechtl and J. Bohdansky, "Sputtering behavior of graphite and molybdenum at low bombarding energies," *Journal of Nuclear Materials*, vol. 123, no. 1, pp. 1431–1436, 1984, doi: https://doi.org/10.1016/0022-3115(84)90280-0.

[9] K. Nishii, S. Clark, H. Tran, D. A. Levin, J. Rovey, and H. B. Chew, "Carbon Sputtering and Transportation in a Ground Facility during Electric Propulsion Testing," in *AIAA AVIATION 2022 Forum*, in AIAA AVIATION Forum. , American Institute of Aeronautics and Astronautics, 2022. doi: doi:10.2514/6.2022-3497.

[10] E. A. Viges, B. A. Jorns, A. D. Gallimore, and J. P. Sheehan, "University of Michigan's upgraded large vacuum test facility," in *36th International Electric Propulsion Conference*, 2019, pp. 1–18.

[11] G. Sabiston and R. Wirz, "Sputtering Reduction Optimization via Volumetrically Complex Materials," in *Bulletin of the American Physical Society*, APS, 2022.

[12] H. Tran and H. B. Chew, "Transient to steady-state morphology evolution of carbon surfaces under ion bombardment: Monte Carlo simulations," *Acta Mater*, vol. 263, p. 119498, 2024, doi: https://doi.org/10.1016/j.actamat.2023.119498.

[13] M. P. Byrne, P. J. Roberts, and B. A. Jorns, "Coupling of Electrical and Pressure Facility Effects in Hall Effect Thruster Testing," in *37th International Electric Propulsion Conference*, Boston, MA, 2022.
[14] W. Eckstein and R. Preuss, "New fit formulae for the sputtering yield," *Journal of Nuclear Materials*, vol. 320, no. 3, pp. 209–213, 2003.
[15] J. T. Yim, "A survey of xenon ion sputter yield data and fits relevant to electric propulsion spacecraft integration," in *35th International Electric Propulsion Conference*, 2017, pp. 8–12.
[16] W. Hurley *et al.*, "Methods for Mitigating Backsputter in Electric Propulsion Test Facilities II: Beam Halter Demonstration during Hall Thruster Testing," in *AIAA SciTech*, Orlando, Florida, 2024.
[17] C. C. Farnell, S. J. Thompson, and J. D. Williams, "Additive Manufacturing for Ion Optics," in *37th International Electric Propulsion Conference*, Boston, Massachusetts, 2022.
[18] E. Pencil, T. Randolph, and D. Manzella, "End-of-life stationary plasma thruster far-field plume characterization," in *32nd Joint Propulsion Conference and Exhibit*, 1996, p. 2709.
[19] W. Huang and R. Shastry, "Analysis of Wien filter spectra from Hall thruster plumes," *Review of Scientific Instruments*, vol. 86, no. 7, p. 073502, Jul. 2015, doi: 10.1063/1.4923282.
[20] W. Huang, R. Shastry, G. C. Soulas, and H. Kamhawi, "Fairfield Plume Measurement and Analysis on the NASA-300M and NASA-300MS," in *International Electric Propulsion Conference (IEPC)*, 2013.
[21] S. J. Thompson, S. C. Farnell, C. C. Farnell, C. C. Farnell, T. M. Andreano, and J. D. Williams, "Combined electrostatic analyzer—Wien filter probe for characterization of species distributions in Hall thrusters," *J Appl Phys*, vol. 130, no. 23, p. 233302, Dec. 2021, doi: 10.1063/5.0071656.
[22] J. S. Miller, S. H. Pullins, D. J. Levandier, Y. Chiu, and R. A. Dressler, "Xenon charge exchange cross sections for electrostatic thruster models," *J Appl Phys*, vol. 91, no. 3, pp. 984–991, Jan. 2002, doi: 10.1063/1.1426246.
[23] M. L. Hause, B. D. Prince, and R. J. Bemish, "Krypton charge exchange cross sections for Hall effect thruster models," *J Appl Phys*, vol. 113, no. 16, p. 163301, Apr. 2013, doi: 10.1063/1.4802432.
[24] A. P. Yalin, J. D. Williams, V. Surla, and K. A. Zoerb, "Differential sputter yield profiles of molybdenum due to bombardment by low energy xenon ions at normal and oblique incidence," *J Phys D Appl Phys*, vol. 40, no. 10, p. 3194, 2007.
[25] J. Williams, M. Johnson, and D. Williams, "Differential sputtering behavior of pyrolytic graphite and carbon-carbon composite under xenon bombardment," in *40th AIAA/ASME/SAE/ASEE Joint Propulsion Conference and Exhibit*, 2004, p. 3788.
[26] Z. L. Zhang and L. Zhang, "Anisotropic angular distribution of sputtered atoms," *Radiation Effects and Defects in Solids*, vol. 159, no. 5, pp. 301–307, 2004.
[27] Q. Wei, K.-D. Li, J. Lian, and L. Wang, "Angular dependence of sputtering yield of amorphous and polycrystalline materials," *J Phys D Appl Phys*, vol. 41, no. 17, p. 172002, 2008.
[28] T. M. Andreano, "Performance and plume characterization of a laboratory krypton Hall thruster," 2020.